Journal of Hydrology 569 (2019) 278–290

Contents lists available at ScienceDirect

Journal of Hydrology

journal homepage: www.elsevier.com/locate/jhydrol

Research papers

Stochastic modeling of oscillatory pumping in heterogeneous aquifers with application to Boise aquifer test

Kan Bun Cheng*, Avinoam Rabinovich, Gedeon Dagan

Faculty of Engineering, School of Mechanical Engineering, Tel-Aviv University, Tel-Aviv, Israel

ARTICLE INFO

This manuscript was handled by Peter K. Kitanidis, Editor-in-Chief, with the assistance of Chunhui Lu, Associate Editor

Keywords:
Oscillatory pumping
Stochastic modelling
Stochastic inversion
Boise aquifer
Aquifer characterization

ABSTRACT

Oscillatory pumping tests consist of injecting periodic discharge into an aquifer and measuring head response along vertical piezometers surrounding the well. The aim is to identify the specific storativity s and conductivity K of the aquifer, which are generally spatially variable. Recently, an analytical solution for oscillating head in a homogeneous formation was derived and applied to the Boise aquifer test site (Rabinovich et al., 2015). Equivalent properties s_{eq}, K_{eq} were identified by best fit of the computed and measured heads. Here, this approach is generalized for heterogeneous aquifers of spatially variable logconductivity ($Y = \ln K$), which is modeled as a stationary space random function characterized by K_G (geometric mean), σ_Y^2 (variance), I and I_v (horizontal and vertical integral scales). Semi-analytical solutions are obtained for the mean head amplitude ($\langle |H| \rangle$) and phase by a first order approximation in σ_Y^2. Application to a given realization requires a large ratio between the well length and I_v, as well as availability of a large number of measurements (ergodicity). We define a correction term, ψ, representing the impact of heterogeneity on $\langle H \rangle$. Investigating the dependence of ψ upon the distance from the pumping well reveals the existence of a few regimes, namely a near well region in which it is independent of period and far away, where the solution pertains to a homogeneous aquifer of effective properties. The solution is applied to the Boise aquifer test by a best fit of $\langle |H| \rangle$ with the measured head in 3 piezometers, for a given value of $\sigma_Y^2 = 0.5$. In spite of the departure from ergodicity, the identification of K_G is quite robust and in agreement with previous tests while that of I is subject to uncertainty. An additional method for improving the identification of K by conditioning on measured point-wise head (co-kriging) is also outlined.

1. Introduction

An oscillatory pumping test is a technique which is drawing increased attention as an alternative to the common continuous pumping test (Hollaender et al., 2002; Rasmussen et al., 2003; Renner and Messar, 2006; Cardiff et al., 2013a; Bakhos et al., 2014; Cardiff and Barrash, 2015; Guiltinan and Becker, 2015; Marco et al., 2018). The procedure consists of injecting a time periodic discharge through a pumping well and measuring head response by pressure sensors in surrounding piezometers. The aim is to identify the aquifer properties (storativity, conductivity) distribution in space by solving an inverse problem. The main advantages are the absence of net discharge (which is especially significant in case of polluted aquifers) and the possibility to pump at different frequencies (allowing to measure head response at larger zones surrounding the well with decreasing frequency). This has led to the suggestion of considering the method as a potential "hydraulic tomography" tool (Gottlieb and Dietrich, 1995; Yeh and Liu, 2000; Bakhos et al., 2014).

The inversion approach followed generally in the literature was deterministic and numerical. In essence, the equations of flow were discretized and the properties at the spatial nodes (conductivity K and storativity s) were regarded as unknowns to be determined as function of the known heads at the measurement points (Kitanidis, 1996; Cardiff et al., 2012). While the procedure has shown promise, it is computationally demanding and poses problems of identifiability, as it is known from the vast literature on the inverse problem (Yeh, 1986; McLaughlin and Townley, 1996; Carrera et al., 2005).

The procedure adopted here is different and it follows the traditional one pursued for continuous pumping: the forward problem for the hydraulic head is solved for given boundary and initial conditions in terms of a few parameters (e.g., K, s). Subsequently, they are determined by a best fit with measured heads. Such a solution for a partially penetrating well of oscillating discharge in a homogeneous and anisotropic formation of finite thickness was presented by Dagan and Rabinovich (2014). The present paper extends the solution to heterogeneous aquifers of spatially variable properties along the stochastic

* Corresponding author.
E-mail address: kanbuncheng@post.tau.ac.il (K.B. Cheng).

https://doi.org/10.1016/j.jhydrol.2018.11.045
Received 19 August 2018; Received in revised form 8 November 2018; Accepted 16 November 2018
Available online 24 November 2018

approach (e.g. Indelman, 2001; Dagan and Lessoff, 2011). The formation properties (primarily the hydraulic conductivity $K(\mathbf{x})$) are regarded as a realization of a stationary space random function which is characterized by a few statistical moments (mean, variance, integral scales). Then, the approach is to solve the forward problem and to arrive at the dependence of the head moments (amplitude and phase) on those of the properties as well as on the frequency. Subsequently the property moments may be determined in principle by a best fit with the observed heads. Although the objectives are more modest than those pursued by a full inversion, the current approach should prove helpful in understanding the processes and forms a starting point for obtaining more general solutions as well as benchmarking numerical solutions. This solution is underlain by restricting assumptions like those of stationarity, of a priori selected statistical structure (e.g. multi-Gaussianity) and of ergodic properties (the possibility to identify moments of the ensemble from the one realization, requiring availability of sufficient data).

The acid test of any method is its application to an actual pumping test for which properties were determined independently. Such an opportunity is offered by the numerous tests conducted at the Boise aquifer site for continuous pumping (e.g. Barrash and Clemo, 1999, 2002; Barrash et al., 2006). These served as field experiments for deterministic inversion (Kitanidis, 1996; Cardiff et al., 2012, 2013a,b). In the context of oscillatory pumping tests, an experiment was recently conducted at the Boise site and the solution for a homogeneous aquifer was used in order to arrive at the equivalent values of the properties (Rabinovich et al., 2015).

In the present study we derive the solution of the mean head for a heterogeneous aquifer by a first order approximation in the logconductivity variance and we shall examine its applicability to the Boise aquifer test. The steps we follow, which constitute the plan of the paper, are: (i) derivation of the basic solution of the mean head for a point source of oscillating strength in an unbounded space domain and isotropic heterogeneity; (ii) generalizations for anisotropic media, for line source and confined aquifer of finite thickness; (iii) examination of the local impact of a head measurement on the mean and variance of the logconductivity by co-kriging and (iv) application to the Boise experiment.

2. Definitions and mathematical statement of the problem

2.1. General

We follow the definitions and formulation of Dagan and Rabinovich (2014) extended to a random heterogeneous medium. Flow is governed by the equation

$$s\frac{\partial H_t}{\partial t} - \nabla\cdot(K\nabla H_t) = 0 \tag{1}$$

where $H_t(\mathbf{x}, t)$ is the head, $\mathbf{x}(x, y, z)$ is a Cartesian coordinate, t is the time, s is the specific storativity (assumed to be constant due to its small variability) and $K(\mathbf{x})$ is the spatially variable hydraulic conductivity (for a homogeneous and isotropic aquifer K is constant). The aquifer is assumed to be unbounded horizontally and of thickness D, such that $-D < z < 0$. The pumping well of length L is located at $x = 0, y = 0$ and along $-D_w < z < -D_w + L$ (Fig. 1).

Flow is driven by a time periodic discharge $Q_w e^{i\omega t}$ where $Q_w = Q_{w,total}/L$ is constant and real, $\omega = 2\pi/T$ is the frequency and T the period. We assume that pumping takes a sufficient time so that $H_t = H(\mathbf{x})e^{i\omega t}$ is also harmonic (the transient period is discussed by Bakhos et al. (2014)). The complex H (the phasor) can be written as $H = |H|e^{i\phi}$ where $\phi(\mathbf{x})$ is the phase. While it is convenient to operate with H, in applications the real part $H_{tR} = |H|\cos(\omega t + \phi)$ is to be used. For a well radius of $r_w \ll L$, we replace the well by distributed sources

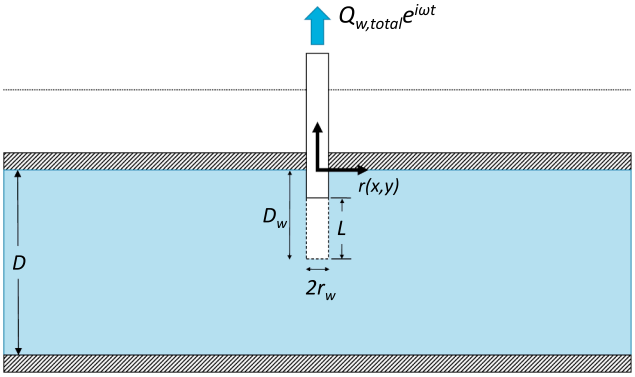

Fig. 1. Definition sketch for a partially penetrating well in a confined aquifer.

of strength $q_w(z)$ such that $Q_w = (1/L)\int_{-D_w}^{-D_w+L} q_w(z')dz'$. Then the equation satisfied by H_t including the well boundary condition becomes

$$s\frac{\partial H_t}{\partial t} - \nabla\cdot(K\nabla H_t) = -e^{i\omega t}\left[\int_{-D_w}^{-D_w+L} q_w(z')\delta(z-z')dz'\right]\delta(x)\delta(y), \tag{2}$$

to be supplemented by the boundary conditions $H \to 0$, $R \to \infty$ and $\partial H/\partial z = 0$ for $z = 0, -D$, pertaining to a confined aquifer (the impact of a phreatic boundary condition is discussed in Rabinovich et al. (2015)).

We model $Y = \ln K(\mathbf{x})$ as a stationary space random function of mean $\langle Y\rangle = \ln K_G$ (where $\langle\ \rangle$ stands for ensemble averaging and K_G is the geometric mean) and variance σ_Y^2. As usual, the two point covariance, of axisymmetric anisotropy, $C_Y = \langle Y'(\mathbf{x})Y'(\mathbf{x}+\xi)\rangle = \sigma_Y^2\rho(\xi')$ depends on $\xi' = \left[(\xi_x^2 + \xi_y^2)/I^2 + \xi_z^2/I_v^2\right]^{1/2}$, where $Y' = Y - \langle Y\rangle$, $\boldsymbol{\xi}$ is the lag vector, ρ is the auto-correlation and I, I_v are the horizontal and vertical integral scales, respectively.

For a heterogeneous aquifer the flux along the well q_w is variable and proportional to $K(0, 0, z)/\overline{K}$, where $\overline{K} = (1/L)\int_{-D_w}^{-D_w+L} K(0, 0, z')dz'$. This boundary condition approximately ensures that the head is uniform along the well screen (Indelman and Dagan, 2004; Firmani et al., 2006). For $L \gg I_v$, $\overline{K} \cong K_A$, the arithmetic mean (see Section 4 for a discussion).

Thus, with $H_t = He^{i\omega t}$, $q_w = (Q_w)[K(0, 0, z)/\overline{K}]$ and $K = K_G e^{Y'}$ substituted in (2) and after division by K and taking into account that $[1/K(x, y, z)]\delta(z - z')\delta(x)\delta(y) = [1/K(0, 0, z')]\delta(z - z')\delta(x)\delta(y)$, the equation satisfied by the phasor H becomes

$$\frac{i\omega s}{K_G e^{Y'}}H - \nabla^2 H - \nabla Y'\cdot\nabla H = -\frac{Q_w}{\overline{K}}\left[\int_{-D_w}^{-D_w+L}\delta(z-z')dz'\right]\delta(x)\delta(y). \tag{3}$$

The mathematical statement of the problem is then: derive the statistical moments of the random H satisfying (3) in terms of those of Y. This is a difficult problem which was solved by Monte Carlo simulations for steady flow ($\omega = 0$) and a fully penetrating well (e.g. Firmani et al., 2006). Here we pursue a well known approximate approach, namely a perturbation expansion $H = H_0 + H_1 + H_2 + \ldots$ where $H_0 = O(1)$, $H_1 = O(Y')$, $H_2 = O(Y'^2)$, ..., presumably applying to weak heterogeneity ($\sigma_Y^2 < 1$). Toward expanding (3) in power series in Y' we rewrite it as follows (see a similar derivation for continuous pumping in Dagan and Lessoff (2011))

$$\begin{aligned}&\tfrac{i\omega s}{K_G}(1 - Y' + \tfrac{Y'^2}{2})(H_0 + H_1 + H_2) - \nabla^2(H_0 + H_1 + H_2)\\ &\quad - \nabla Y'\cdot\nabla(H_0 + H_1 + H_2)\\ &= -\tfrac{Q_w}{\overline{K}}\left[\int_{-D_w}^{-D_w+L}\delta(z-z')dz'\right]\delta(x)\delta(y).\end{aligned}$$

Collecting terms of same order in Y' leads to a sequence of Poisson equations for H_j as follows

$$\frac{\gamma^2}{K_G}H_j - \nabla^2 H_j = \eta_j(\mathbf{x}) \qquad (j = 0, 1, 2, ...) \tag{4}$$

$$\eta_0 = -\frac{Q_w}{\overline{K}}\left[\int_{-D_w}^{-D_w+L} \delta(z-z')dz'\right]\delta(x)\delta(y)$$

$$\eta_1 = \nabla Y'\cdot\nabla H_0 + \frac{\gamma^2}{K_G}Y'H_0$$

$$\eta_2 = \nabla Y'\cdot\nabla H_1 + \frac{\gamma^2}{K_G}Y'H_1 - \frac{\gamma^2}{K_G}\frac{Y'^2}{2}H_0,$$

where $\gamma = (i\omega s)^{1/2} = (1+i)(\omega s/2)^{1/2}$ is assumed to be constant. Eq. (4) is supplemented with the boundary conditions $\partial H_j/\partial z = 0$ for $z = 0, -D$. It is seen that $H_0 = -(Q_w/\overline{K})h_0(\mathbf{x})$ is deterministic and represents the solution of flow in a homogeneous aquifer solved by Dagan and Rabinovich (2014). Furthermore, $\langle H_1\rangle = 0$ (since η_1 is linear in Y'), while $\langle H_2\rangle = (Q_w/\overline{K})\langle h_2(\mathbf{x})\rangle$ is proportional to σ_Y^2 (since η_2 is quadratic in Y').

The main aim of the paper is to derive H_j ($j = 0, 1, 2$) and primarily the first order approximation in σ_Y^2 of the mean head $\langle H\rangle = (Q_w/\overline{K})[h_0 + \langle h_2\rangle]$. While the quantitative result may be valid for weak heterogeneity, the analysis may help to grasp the major features of the solution in general.

2.2. Formulation by the Green's Function

Following the steps of Dagan and Rabinovich (2014) we pursue the general solution of (4) with the aid of the Green's function in an infinite domain which satisfies

$$\frac{\gamma^2}{K_G}G - \nabla^2 G = -\delta(x-x')\delta(y-y')\delta(z-z')$$

$$\text{of solution } G(r) = -\frac{1}{4\pi r}e^{-\frac{\gamma r}{\sqrt{K_G}}}, \tag{5}$$

where $r = |\mathbf{x}-\mathbf{x}'|$ (Carslaw and Jaeger, 1959). We shall also use the dimensionless complex parameter $\alpha = \gamma I/\sqrt{K_G} = (i\omega s)^{1/2}I/K_G$ such that in (5) $G(r) = -(4\pi r)^{-1}\exp(-\alpha r/I)$.

Then the general solution of (4) in an infinite domain can be written as follows

$$H_j(\mathbf{x}) = \int_{-\infty}^{\infty}\int_{-\infty}^{\infty}\int_{-\infty}^{\infty}\eta_j(\mathbf{x}'')G(\mathbf{x}-\mathbf{x}'')d\mathbf{x}''. \tag{6}$$

To satisfy the boundary conditions on $z = 0, -D$ we need to supplement G by the appropriate images across the boundary. Thus, for a confined aquifer the total Green's function is given by

$$G_t(\mathbf{x},\mathbf{x}') = \sum_{m=-\infty}^{m=\infty} G(|\mathbf{R}-\mathbf{R}'|, |z-z'-2mD|) + G(|\mathbf{R}-\mathbf{R}'|, |z+z'-2mD|)\Big), \tag{7}$$

where the vector $\mathbf{R}(x, y)$ is a planar coordinate such that $|\mathbf{R}-\mathbf{R}'| = [(x-x')^2 + (y-y')^2]^{1/2}$.

Thus, the solution for h_0 in the expression $H_0 = -(Q_w/\overline{K})h_0$ is obtained by plugging (7) in (6) with η_0 from (4), and given by

$$h_0 = \int_{-D_w}^{-D_w+L} G_t(x, y, z-z')dz'. \tag{8}$$

If we substitute $\overline{K} = K_G$, this is precisely the solution of Dagan and Rabinovich (2014), Rabinovich et al. (2015) for a homogeneous aquifer of conductivity K_G. Thus h_0 (8) is defined in the entire space as a line source over the well supplemented by the appropriate reflections across the boundaries $z = 0, -D$.

In a similar manner we arrive at

$$\langle h_2\rangle = \int_{-\infty}^{\infty}\int_{-\infty}^{\infty}\int_{-\infty}^{\infty}\left\{[\langle\nabla Y'\cdot\nabla h_1\rangle + \frac{\gamma^2}{K_G}\langle Y'h_1\rangle]_{\mathbf{x}=\mathbf{x}'} - \frac{\gamma^2}{K_G}\frac{\sigma_Y^2}{2}h_0(\mathbf{x}')\right\} \cdot G_t(\mathbf{x}-\mathbf{x}')dx'dy'dz', \tag{9}$$

which satisfies (6), leading at first order to $\langle H\rangle = H_0 + \langle H_2\rangle = -(Q_w/\overline{K})(h_0 + \langle h_2\rangle)$; see Dagan and Lessoff (2011) for a similar development for phreatic heterogeneous aquifers. In the following we concentrate on deriving $\langle h_2\rangle$ by integration in (9).

3. The basic solution for a unit source in an unbounded domain

3.1. General

It is seen that h_0 (8) is a summation of sources of unit strength along the well axis and h_1, h_2 are linear in h_0 (Eq. (4)). Thus the basic solution contributing to $H_0 = -(Q_w/\overline{K})h_0$ is given by

$$H_{0s} = -(Q_w/\overline{K})h_{0s}, \quad h_{0s} = G(x, y, z-z')$$
$$\text{and } H_0 = \int_{-D_w}^{-D_w+L} H_{0s}dz', \tag{10}$$

where H_{0s} is dimensionless while h_{0s} is length^{-1}.

Subsequently, the first order correction to h_{0s} becomes

$$h_{1s} = \int\left[-\nabla Y'\cdot\nabla h_{0s} + \frac{\gamma^2}{K_G}Y'h_{0s}\right]_{\mathbf{x}=\mathbf{x}'} G(\mathbf{x}-\mathbf{x}')d\mathbf{x}', \tag{11}$$

with integration over the entire space.

In order to arrive at $\langle h_{2s}\rangle$ we have to plug h_{0s} (10) and h_{1s} (11) in (9) and average. The detailed computations are given in Appendix A, leading to the final expression (A.8) which is reproduced here

$$\frac{\langle h_{2s}(\mathbf{x}')\rangle I}{\sigma_Y^2} = \left\{\int d\mathbf{y}'\left[\frac{d^2\rho(\xi')}{d\xi'^2}\frac{(1+y'\sqrt{\alpha})(\mathbf{x}'\cdot\mathbf{y}'-y'^2)}{y'^2|\mathbf{x}'-\mathbf{y}'|} + \frac{d\rho(\xi')}{d\xi'}\frac{\sqrt{\alpha}(1+y'\sqrt{\alpha})}{y'} + \frac{d\rho(\xi')}{d\xi'}\frac{\alpha(\mathbf{x}'\cdot\mathbf{y}'-y'^2)}{|\mathbf{x}'-\mathbf{y}'|} - \rho(\xi')\alpha^{3/2}\right]\left[\frac{e^{-y'\sqrt{\alpha}}}{4\pi y'}\right]\left[\frac{e^{-\sqrt{\alpha}|\mathbf{x}'-\mathbf{y}'|}}{8\pi}\right]\right\} + \frac{\sqrt{\alpha}}{2}\left[\frac{e^{-\sqrt{\alpha}|\mathbf{x}'|}}{8\pi}\right], \tag{12}$$

where $\mathbf{y}' = \mathbf{y}/I$, $\mathbf{x}' = \mathbf{x}/I$, $\xi' = (y_1'^2 + y_2'^2 + y_3'^2/f^2)^{1/2}$ and $f = I_v/I$.

The general solution for $\langle h_{2s}\rangle$ is seen to depend on the logconductivity autocorrelation ρ, which has to be specified. The computation requires 3 quadratures for an anisotropic axi-symmetric ρ and 2 for isotropic ρ. The solution generalizes the one for steady flow ($\alpha = 0$) obtained by Dagan and Lessoff (2011) and by Severino et al. (2008). In the following we proceed with application to isotropic and anisotropic media for Gaussian and exponential logconductivity autocorrelations ρ.

Toward this aim it is convenient to operate with the complex function $\psi(\mathbf{x}) = \langle H_2\rangle/(\sigma_Y^2 H_0) = \langle h_2\rangle/(\sigma_Y^2 h_0)$ such that at first order $\langle H\rangle = (Q_w/\overline{K})\,h_0(1+\sigma_Y^2\psi)$ (see e.g. IIndelman and Abramovich, 1994; Severino et al., 2008; Dagan and Lessoff, 2011). Hence, the dimensionless $\psi(\mathbf{x})$ represents the effect of heterogeneity on the solution $\langle H\rangle$. For a unit source and an infinite, isotropic medium, ψ_s is a function of r/I and α, where $r = [x^2 + y^2 + (z-z')^2]^{1/2}$.

3.2. Isotropic media

The complex $\psi_s = \psi_{s,R} + i\psi_{s,I}$ function has been computed by 2 quadratures in Appendix A for a Gaussian and an exponential ρ, respectively,

$$\rho_G = \exp(-\pi\xi'^2/4), \quad \rho_E = \exp(-\xi'). \tag{13}$$

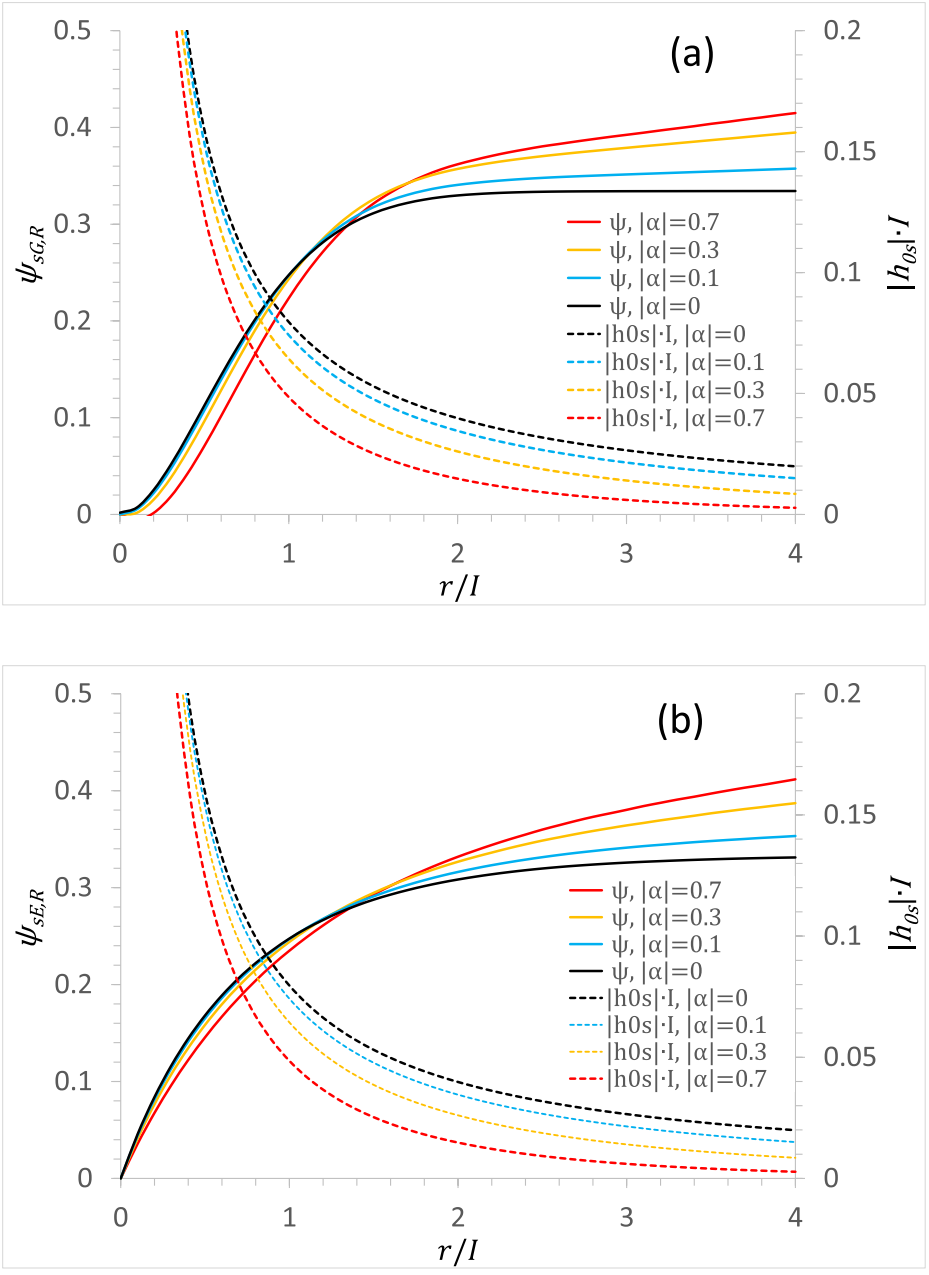

Fig. 2. The functions ψ (real part) for (a) Gaussian, and (b) exponential auto-correlations and $|h_{0s}|\cdot I$ (Eqs. (12) and (14)) as function of dimensionless distance from a point source.

Starting with the amplitude of $\langle h_s \rangle = h_{0s}(1 + \sigma_Y^2 \psi_s)$ we can write at first order $|\langle h_s \rangle| = |h_{0s}|(1 + \sigma_Y^2 \psi_{s,R})$, where $\psi_{s,R}$ is the real part of ψ_s. Indeed, $|(1 + \sigma_Y^2 \psi_s)| = [(1 + \sigma_Y^2 \psi_{s,R})^2 + \sigma_Y^4 \psi_{s,I}^2]^{1/2} = 1 + \sigma_Y^2 \psi_{s,R} + 0(\sigma_Y^4)$. In Fig. 2a and b we have depicted $\psi_{sG,R}$ and $\psi_{sE,R}$, the real part of ψ_s for a Gaussian and exponential auto-correlation respectively, as functions of r/I and for a few values of the dimensionless parameter $|\alpha| = |\gamma| I/\sqrt{K_G} = (\omega s)^{1/2} I/\sqrt{K_G}$. The selected range is $0 < |\alpha| < 0.7$, i.e., between steady state and the highest considered frequency which was found to be compatible with common data. Similarly, the displayed range of distance is $0 < r/I < 4$, since the solution $|h_{0s}|$ decays exponentially with distance for $|\alpha| > 0$ and it is negligible for $r/I > 4$, as illustrated in Fig. 2.

Starting with the steady state ($\gamma = 0 \rightarrow \alpha = 0$), $h_{0s} = G = -1/(4\pi r)$, analytical solutions were derived in the past (Dagan and Lessoff, 2011; Severino et al., 2008) for ψ_s, which is real

$$\psi_{sG} = \frac{1}{3}\left[1 - \left(1 - \frac{\pi}{2}\right)\left(\frac{r}{I}\right)^2 e^{-\frac{\pi}{4}\left(\frac{r}{I}\right)^2} + \frac{\pi^2}{4}\left(\frac{r}{I}\right)^3 \mathrm{erfc}\left(\frac{\sqrt{\pi}}{2}\frac{r}{I}\right)\right] \tag{14}$$

$$\psi_{sE} = \frac{1}{3}\left[1 - \left(1 - \frac{(r/I)}{2} + \frac{(r/I)^2}{2}\right)e^{-(r/I)} + \frac{(r/I)^3}{2}\mathrm{Ei}\left(-\frac{r}{I}\right)\right]$$

for Gaussian and Exponential ρ (13), respectively. The discussion of the results by Dagan and Lessoff (2011) is retaken here briefly. It is seen (Fig. 2, full lines) that the solution (14) is made up from two parts: the near field (for $r/I < r_A/I$) and the far field (for $r/I > r_A/I$), where $r_A/I \cong$ 2, 3 for the Gaussian and Exponential ρ, respectively. In the near field $\psi_{sG,E}$ are seen to grow from zero up to $\psi_{sG,E} = 1/3$ and they remain constant for $r > r_A$.

The results in Fig. 2 for steady state were interpreted by Dagan and Lessoff (2011) as follows. Limiting here the discussion to the far field, the solution pertains to a homogeneous medium of effective

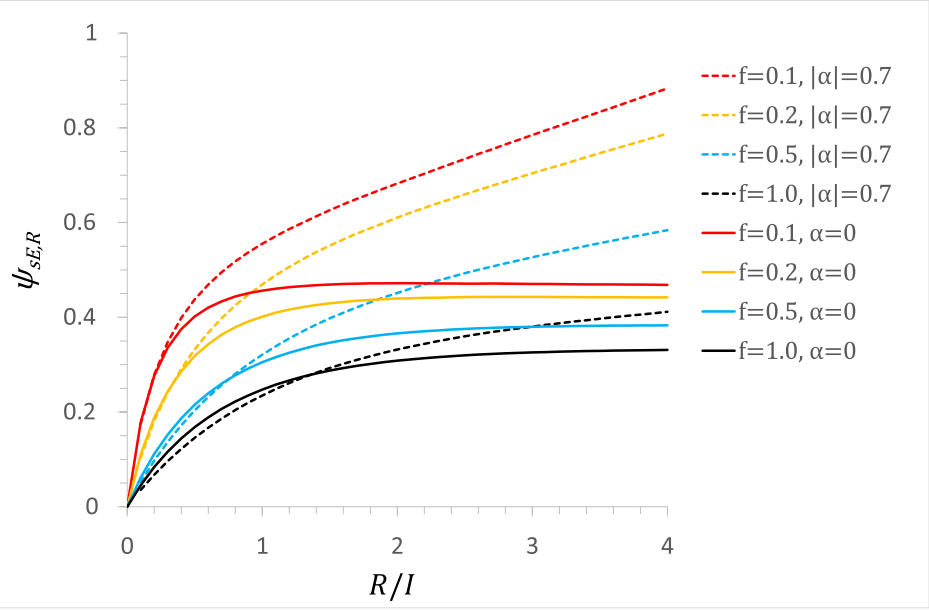

Fig. 3. The function ψ (real part, Eq. (12)) for anisotropic media as function of dimensionless horizontal distance from a point source (exponential auto-correlation) for various values of anisotropy ratio ($f = I_v/I$).

conductivity in uniform flow $K_{ef} = K_G(1 + \sigma_Y^2/6)$. Indeed, with $\langle H_s\rangle = -(Q_w/\overline{K})h_{0s}(1 + \sigma_Y^2\psi_s)$ and for $\overline{K} \cong K_A = K_G(1 + \sigma_Y^2/2)$ and $\psi_s = 1/3$ we arrive at first order at $\langle H_s\rangle = -(Q_w/K_G)h_{0s}(1 - \sigma_Y^2/6)$. This is precisely the first order expansion of $\langle H_s\rangle = -(Q_w/K_{ef})h_{0s}$ with $h_{0s} = -1/(4\pi r)$.

We move now to the main objective of the present paper, namely the computation of $\langle H_s\rangle$ for oscillatory pumping ($\gamma \neq 0$). With $\langle H_s\rangle = -(Q_w/\overline{K})(h_{0s} + \langle h_{2s}\rangle) = -(Q_w/\overline{K})h_{0s}(1 + \sigma_Y^2\psi_s)$ where both h_{0s} and ψ_s are complex, we start with the amplitude. As already mentioned above, at first order it is given by $|\langle H_s\rangle| = (Q_w/\overline{K})|h_{0s}|(1 + \sigma_Y^2\ \psi_{s,R})$, where $|h_{0s}| = |G| = \frac{1}{(4\pi r)}\exp[-(|\gamma|/\sqrt{2K_G})r]$ and $|\gamma| = (\omega s)^{1/2}$. In Fig. 2a and b we have plotted $\psi_{sG,R}$ (for Gaussian ρ_G) and $\psi_{sE,R}$ (for Exponential ρ_E) derived from (12) as functions of r/I for a few values of $0 < |\alpha| < 0.7$.

We may discern now the existence of three zones: (i) a near zone $0 < r/I < r_A/I\,(r_A/I \cong 1.5)$ for which the unsteady $\psi_{s,R}$ is close to the steady one for the examined $|\alpha|$ range. In words, heterogeneity correction is not affected by unsteadiness (which nevertheless impacts $|h_{0s}|$), the solution for a homogeneous medium (see Fig. 2); (ii) an intermediate zone $r_A/I < r/I < r_B/I$ for which $\psi_{s,R}$ is non-linear and larger than the steady one ($r_B/I \cong 2.5$) and (iii) an asymptotic zone $r/I > r_B/I$ in which $\psi_{s,R}$ grow linearly with r/I with a slope depending on $|\alpha|$ but not on r/I or the ρ shape. The values of r_A/I, r_B/I are approximately estimated from direct inspection of Fig. 2.

Although the asymptotic zone is of limited interest in applications due to the fast drop of the leading term $|h_{0s}|$ with r (Fig. 2), it is of theoretical interest to discuss it. Thus, in the terminology of the literature on perturbation expansions, the expression $1 + \sigma_Y^2\psi_{s,R}$ is non-uniform since no matter how small is σ_Y^2, for a sufficiently large r the second term becomes larger than unity. The computations based on (12) show that the constant slope is given approximately by $|\alpha|/12\sqrt{2}$ for $|\alpha| \lesssim 0.3$ but somewhat smaller for larger $|\alpha|$; however the leading term $|h_{0s}|$ drops to very small values for $|\alpha| > 0.3$ and $r/I > 4$ (Fig. 2) making it again of little relevance to applications. The result for sufficiently low frequencies $|\alpha| \lesssim 0.3$ can be explained similarly to the one pertaining to steady state: far from the source the solution is the one prevailing in a homogeneous medium of effective conductivity in mean uniform flow K_{ef}. Indeed with $|\langle H_s\rangle| = (Q_w/K_{ef})(4\pi r)^{-1}\exp[-(|\gamma|r/\sqrt{2K_{ef}})]$ and $K_{ef} = K_G(1 + \sigma_Y^2/6)$, expansion of the exponential term leads to $\exp[-(|\gamma|r/\sqrt{2K_{ef}})] = \exp\{-[|\alpha|/\sqrt{2(1 + \sigma_Y^2/6)}](r/I)] = \exp[-(|\alpha|/\sqrt{2})(r/I)]\cdot[1 + \sigma_Y^2(|\alpha|/12\sqrt{2})(r/I)]$ and indeed the slope of $\psi_{s,R}$ is $|\alpha|/12\sqrt{2}$.

Moving now to the phase of $\langle h_s\rangle = h_{0s}(1 + \sigma_Y^2\psi_s)$, the argument of $\langle h_s\rangle$ is given at first order by $\arg[h_{0s}] + \sigma_Y^2\psi_{s,\mathrm{Im}}$. The detailed computation based on (12) led to the maximal value $\psi_{s,\mathrm{Im}} \lesssim 0.2\arg[h_{0s}]$ for $r/I < 4$ and $|\alpha| \lesssim 0.7$. Therefore, the impact of heterogeneity on the phase is quite low and the isotropic aquifer can be regarded as homogeneous for phase estimation.

3.3. Anisotropic media

It is reminded that statistical anisotropy is related to the existence of different integral scale I, I_v in the horizontal and vertical directions, respectively. The computations leading to the complex $\langle h_{2s}\rangle$ were carried out on the basis of the same general solution (12), but this time with the argument $\xi' = \left[\left(\xi_x^2 + \xi_y^2\right)/I^2 + \xi_z^2/I_v^2\right]^{1/2}$ substituted in ρ (13). The second order correction $\langle h_{2s}\rangle$ which is now a function of $R = (x^2 + y^2)^{1/2}$, $|z - z'|$, γ and $f = I_v/I < 1$, is computed by 3 quadratures in (12). With $h_{0s} = -(4\pi r)^{-1}\{\exp[-(\gamma/\sqrt{K_G})r]\}$ pertaining to a homogeneous medium of conductivity K_G, the correction $\psi_s = \langle h_{2s}\rangle/(\sigma_Y^2 h_{0s})$ becomes also a function of R/I, $(z - z')/I$, $\gamma/\sqrt{K_G}$ and f. Concentrating now on the amplitude $|\langle h_s\rangle|$ we have illustrated in Fig. 3 (similarly to Fig. 2b), the dependence of $\psi_{sE,R}$ on R/I (for $z - z' = 0$) for the extreme values of $|\alpha| = 0$ (steady state) and maximal $|\alpha| = 0.7$ as well as for $f = 0.1$, 0.2, 0.5 and 1 (isotropic medium).

Starting with the steady state ($\alpha = 0$), it is seen that the behaviour for $f < 1$ is similar to the isotropic case: in the near field $R/I < R_A/I$, $\psi_{sE,R}$ grows from zero and stabilizes to a constant. However, the value of R_A decreases with f, i.e. the transition zone is narrower than for $f = 1$. In the far field ($R > R_A$) the analytical expression of the constant $\psi_{sE,R}$ is discussed in the sequel.

Similarly to the isotropic case, for the oscillatory pumping ($|\alpha| > 0$), $\psi_{sE,R}$ as function of R/I displays three zones. In the first one $R/I < R_A/I$ the solution is close to the steady solution; however, its size decreases with the diminishing of the anisotropy ratio f. Then, an intermediate zone $R_A/I < R/I < R_B/I$ with $R_B/I \lesssim 2$, of same behavior of non-linear growth with R/I. Finally, for the asymptotic $R/I > R_B/I$, $\psi_{sE,R}$ grows

linearly with R/I but with slopes depending on both $|\alpha|$ and f.

As for the dependence of $\psi_{sE,R}$ upon $|z-z'|$ for $R=0$, it is of lesser interest in applications since observation wells are always at a finite R. The dependence of $\psi_{sE,R}$ on $z-z'$ for a fixed R can be derived by integration in (12) and it is illustrated in Fig. 5.

Similar to the isotropic case, the plateau values for steady state and the slope for unsteady one, can be determined analytically from the solution of flow in a homogeneous medium of local anisotropic effective conductivity in uniform flow. Toward the derivation, we recall the solution of Dagan and Rabinovich (2014)

$$h'_{0s}=-\frac{1}{4\pi r'}\exp[-\gamma r'/\sqrt{K_{efv}}]$$
$$\text{with } r'=\left[\frac{K_{efv}}{K_{efh}}R^2+(z-z')^2\right]^{1/2} \tag{15}$$

where K_{efh} and K_{efv} are the horizontal and vertical effective conductivities in uniform flow.

Starting with the amplitude $|\langle H_s\rangle|=(Q_w/K_A)|h'_{0s}|$, we plugged in (15) the first order approximations for uniform flow $K_{efh}/K_G=1+(\sigma_Y^2/2)(1-\lambda)$, $K_{efv}/K_G=1+(\sigma_Y^2/2)(2\lambda-1)$, $K_{efv}/K_{efh}=-1+(\sigma_Y^2/2)(3\lambda/2-1)$, $K_A/K_G=1+\sigma_Y^2/2$ where $\lambda=\frac{f^2}{1-f^2}\left[\left(\frac{1}{f\sqrt{1-f^2}}tan^{-1}\sqrt{\frac{1}{f^2}-1}\right)-1\right]$ (Gelhar and Axness, 1983; Dagan, 1989). Subsequently, after replacing K_{efh} and K_{efv} by their first order approximations, we expanded h'_{0s} (15) in a consistent power series in σ_Y^2. Starting with the steady state ($\gamma=0$), the result is identical with the one based on the solution of Dagan and Lessoff (2011, Eq. (48)) and given by $\langle H_s\rangle=(Q_w/K_G)h_{0s}\{1+\sigma_Y^2[(\lambda/2+(1/2-3\lambda/4)(R^2/r^2)]\}$), where $h_{0s}=-1/(4\pi r)$. Hence, from the definition here $\langle H_s\rangle=(Q_w/K_A)h_{0s}\ (1+\sigma_Y^2\psi_s)$, $K_A=K_G(1+\sigma_Y^2/2)$ we get at first-order $\langle H_s\rangle=(Q_w/K_G)h_{0s}\ [1+\sigma_Y^2(\psi_s-1/2)]$ where $\psi_s=\psi_{sE}=\psi_{sG}$ does not depend on the shape of ρ. It is seen by comparing the two expressions that for $z-z'=0$ and $r\to R$, $\psi_s=1/2-\lambda/4$ in the far field and these are the values shown in Fig. 3 (ψ_s varies between 1/3 for $f=1$, $\lambda=2/3$ and 1/2 for $f=0$, $\lambda=0$). A similar far field behavior applies to the dependence of the steady state solution upon $|z-z'|$ for $R=0$ (not shown here).

In a similar vein it is found, for the periodic case, by the expansion of $|h'_{0s}|$ (15) that the slope of the linear part (for $R/I>R_B/I$) is given approximately by $(|\alpha|/4\sqrt{2})(1-\lambda)$ and again these values were found in agreement with those derived by integration (displayed in Fig. 3) for $|\alpha|<0.3$, with slight differences for $0.3<|\alpha|<0.7$. The agreement was found to improve for diminishing f. It is worthwhile to mention that the slopes vary between $|\alpha|/(12\sqrt{2})$ for $f=1$, $\lambda=2/3$ to $|\alpha|/(4\sqrt{2})$ for $f\to 0$, $\lambda=0$. Thus the relative effect of heterogeneity for anisotropic media is larger than for isotropic ones.

Similar trends show up in the solution $\psi_{sG,R}$ for the Gaussian $\rho_G(\xi')$. For illustration we have represented in Fig. 4 the solutions for $\psi_{sG,R}$, $\psi_{sE,R}$ for the extreme cases ($f=0.1$, 1 and $|\alpha|=0$, 0.7) where the solution for $\alpha=0$ and $f=1$ is given explicitly by (14). It is seen that while the solutions are somewhat different for the isotropic media in the first two zones, they become closer.

Similarly to the isotropic, the phase is given at first order by $\arg\langle h_s\rangle=\arg[h_{0s}]+\sigma_Y^2\psi_{s,\mathrm{Im}}$. The ratio $\psi_{s,\mathrm{Im}}/\arg[h_{0s}]$, derived from (12), increases with decreasing f and increasing R/I, still it does not exceed 0.2 for $f=0.1$, $R/I\cong 3$ and $|\alpha|<0.7$. Therefore, the phase is dominated by that of h_{0s} and heterogeneity effect can be generally neglected as far as phase is concerned.

Though in principle the impact of heterogeneity upon the amplitude is reflected by the magnitude of $\sigma_Y^2\ \psi_{s,R}$ relative to unity, what counts is the impact upon the total head $|\langle h_s\rangle|=|h_{0s}|(1+\sigma_Y^2\psi_{s,R})$. Thus, although $\psi_{s,R}$ grows with R/I (Figs. 3 and 4), the heterogeneity effect is quite limited for $\sigma_Y^2<1$, due to the steep drop of $|h_{0s}|$ with r/I (see Fig. 2). For illustration we present in Fig. 5 ($|\alpha|=0.7$, $\sigma_Y^2=0.5$) the dependence of $|\langle h_s\rangle|$ and $|h_{0s}|$ upon $|z-z'|$ (for at a few fixed vertical lines at $R/I=0.5$, 1, 2) and for different f. The selected values for $|\alpha|$, σ_Y^2 and R/I are relevant to the Boise aquifer test discussed in Section 6. At any rate, this is the starting point for comparison with measured heads in piezometers surrounding the pumping well. Fig. 5 reveals a few findings: first, the maximal heterogeneity impact at $|z-z'|=0$ (across the source) occurs for the highest degree of anisotropy $f=0.1$; secondly, both $|\langle h_s\rangle|$ and $|h_{0s}|$ and the difference between them drop with increasing R/I and $|z-z'|$ and can be neglected for practical purposes for say $R/I>2$ and/or $|z-z'|>2$.

We note that heterogeneity may have a larger impact for large σ_Y^2 as shown by the derivation of K_{ef} in 1D flow by Rabinovich et al. (2013), using a different method. The extension of the computation of K_{ef} to 3D well flow is a challenging task still to be pursued in the future.

4. Extension to well of finite length in a confined aquifer

We consider first a well of finite length L (Fig. 1) pumping periodically in an unbounded domain. The zero order approximation h_0 is given by (8), a distribution of sources of unit strength along the well. Due to the linear dependence of the higher order approximations (see Eq. (4)) upon h_0, $\langle h_2\rangle$ is also obtained by an additional integration of the solution $\langle h_{2s}\rangle$ (12) for $\mathbf{x}(x,y,z-z')$ over z' in the interval $-D_w<z'<-D_w+L$ (Fig. 1). The zero order approximation is now obtained by integration over z' in (8) and (5), which requires a numerical quadrature for $|\gamma|>0$. It simplifies for steady state ($\gamma=0$), for which the solution has the well known analytical expression $h_0=\frac{1}{4\pi}ln\left[\frac{D_w-L+z+\sqrt{R^2+(D_w-L+z)^2}}{D_w+z+\sqrt{R^2+(D_w+z)^2}}\right]$. For the periodic flow integration over z' in $\langle h_{2s}\rangle$ (12) requires four quadratures that were carried out numerically. The correction $\psi=\langle h_2\rangle/(\sigma_Y^2h_0)$ is now a function of the additional parameter L/I. For illustration we represent in Fig. 6 the dependence of the real part $\psi_{E,R}$ (exponential covariance) on R/I for the centerline $z=-D_w+L/2$ and for a few values of L/I. This is done for the extreme values $f=0.1$, 1 and $|\alpha|=0.7$. It is reminded that mean head amplitude is given at first order by $|\langle H\rangle|=(Q_w/K_G)|h_0|(1+\sigma_Y^2\psi_R)$. It is seen that the general behaviour is quite similar to that pertaining to a source (see Fig. 3).

The next and last step is to account for the no flow boundary condition $\partial H/\partial z=0$ for $z=0$, $-D$. As already indicated above this is achieved by adding to the solution in an unbounded domain images in the z direction across the boundaries (see Eq. (5)).

Due to the exponential decay of $|H|$ with distance, the number of images required in order to ensure convergence even for large R is smaller than for steady state ($\gamma=0$). To illustrate the impact of boundaries we have depicted in Fig. 7 the dependence of $\psi_{sE,R}$ on R/I in an unbounded domain as well as a bounded one for $|\alpha|=0$, 0.7 and different D/I for a source at the mid-distance $z=-D/2$. It is seen that the presence of the impervious boundaries causes an increase of $\psi_{sE,R}$ relative to the unbounded domain for the smallest $D/I=4$ and is insignificant for $D/I>10$.

At this point it is worthwhile to discuss briefly the issue of ergodicity of the average conductivity $\overline{K}=(1/L)\int K(0,0,z')dz'$ along the pumping well. In the general derivations so far we have assumed that the ratio L/I_v is much larger than unity, to allow exchanging $\overline{K}$ by the arithmetic mean K_A. Numerical simulations (Firmani et al., 2006) for steady flow and a fully penetrating well indicated that ensuring the exchange between $\overline{K}$ and K_A requires a relatively large L/I_v. A similar analysis for oscillating pumping still awaits accurate numerical simulations. At present there are a few avenues for accounting for non-ergodic behavior. First, in absence of additional data, K_A can be regraded as the best estimator of $\overline{K}$, as done here. Alternatively $\overline{K}$ can be regarded as random (Dagan, 1989), of variance depending on L/I_v, a task not undertaken here. If in a field test the values of K were sampled along the well, $\overline{K}$ may be regarded as deterministic and the K distribution in the neighborhood of the well can be derived by conditioning (kriging). This approach, which is straightforward and leads

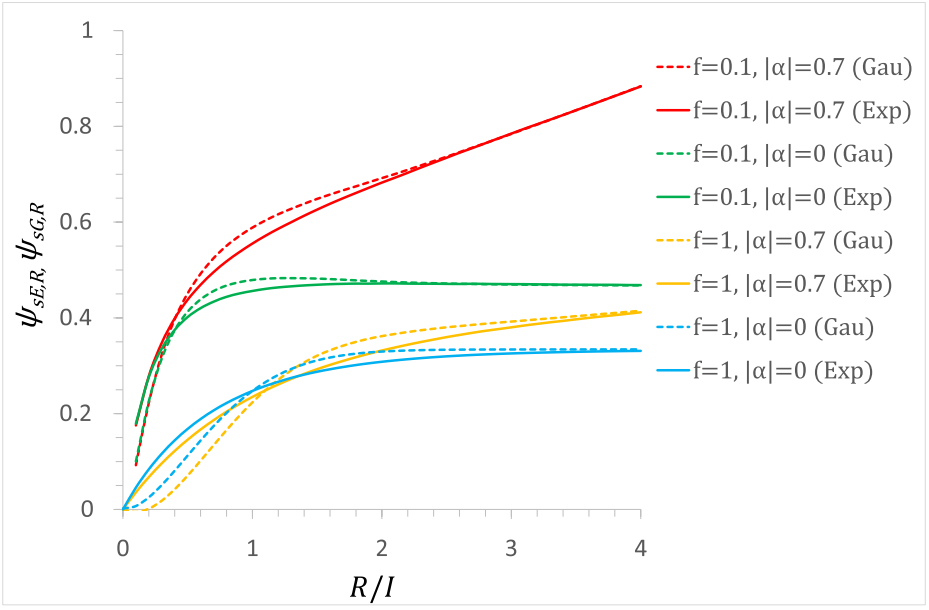

Fig. 4. The function ψ (real part, Eq. (12)) for Gaussian and exponential auto-correlations as function of dimensionless horizontal distance from a point source.

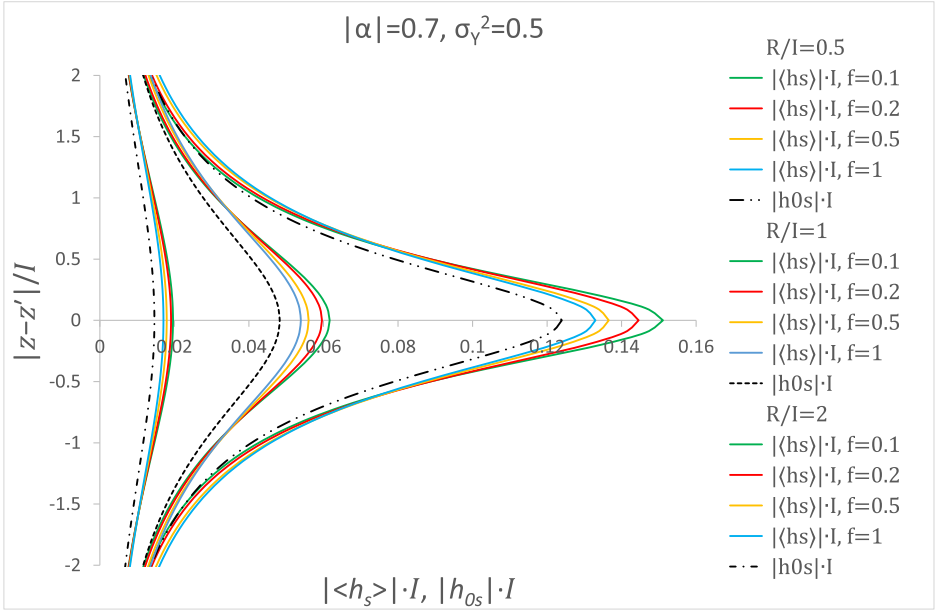

Fig. 5. The vertical head profiles at different horizontal distances (R/I) from a point source for exponential auto-correlation.

to a non-stationary Y field in the neighborhood of the well is not pursued here either.

5. Stochastic inversion by conditional averaging (co-kriging)

The analysis so far focused on the dependence of the mean head upon the parameters characterizing statistically the aquifer structure (K_G, σ_Y^2, I, f). However, hydraulic tomography, as defined and applied in deterministic inversion, has the more ambitious goal of identifying the distribution of the conductivity K in space by using the actual measured values of the head in piezometers surrounding the pumping well.

A similar goal was pursued in the stochastic frame by the inversion procedure proposed for instance by Dagan (1985). The simple idea is to derive first the unconditional covariances $C_{YH}(\mathbf{x}, \mathbf{x}') = \langle Y'(\mathbf{x})|H'(\mathbf{x}')|\rangle$ and $C_H(\mathbf{x}, \mathbf{x}') = \langle|H'(\mathbf{x})H'(\mathbf{x}')|\rangle$, where Y' and $|H'|$ are residuals. This can be achieved in the present case by using the first order solution $H' = H_1 = -(Q_w/\overline{K})h_1$, where for a point source in an unbounded domain h_{1s} is given by (11). Next, assuming that a set of head measurements is available e.g. along vertical piezometers, the logconductivity moments $\langle Y^c(\mathbf{x})\rangle$, $\sigma_Y^{2,c}$ conditioned on measurements are derived by solving first the co-kriging system

$$\sum_{j=1}^{M} \mu_j(\mathbf{x}) C_H(\mathbf{x}_j, \mathbf{x}_k) = C_{YH}(\mathbf{x}, \mathbf{x}_k) \quad (k = 1, \ldots, M), \tag{16}$$

where $\mathbf{x}_j$ are the M points at which head measurements H_j are available. Once the coefficients $\mu_j(\mathbf{x})$ are derived by solving (16), the conditional

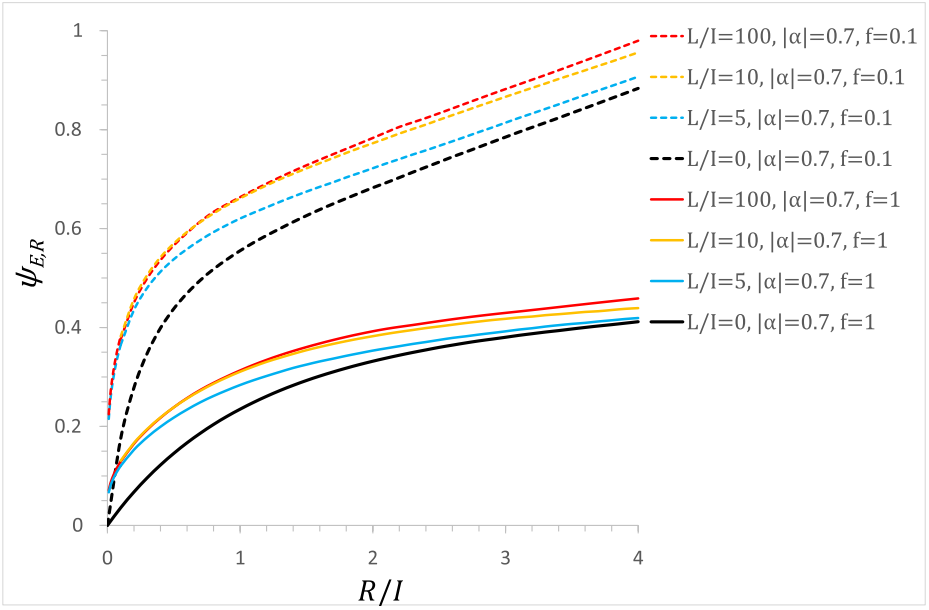

Fig. 6. The function ψ (real part) for exponential auto-correlation as function of dimensionless horizontal distance from the center of a line source in an infinite domain for varying well length (L/I).

logconductivity first two moments are given by

$$\langle Y^c(\mathbf{x})\rangle = \langle Y(\mathbf{x})\rangle + \sum_{j=1}^{M} \mu_j(\mathbf{x}) |H_j'|,$$
$$\sigma_{Y^c}^2(\mathbf{x}) = \sigma_Y^2(\mathbf{x}) - \sum_{j=1}^{M} \mu_j(\mathbf{x}) C_{YH}(\mathbf{x}, \mathbf{x}_j). \tag{17}$$

The procedure was applied by Dagan (1985) to steady two-dimensional mean uniform flow of constant mean head gradient $\mathbf{J} = -\nabla\langle H\rangle$ in an unbounded medium characterized by an unconditional exponential isotropic Y of auto-correlation ρ_E (13). In this case the unconditional covariances C_H and C_{YH} are stationary, depending on $\mathbf{x} - \mathbf{x}'$, and have analytical expressions. The main objective was to examine the impact of reduction of the conditional variance, i.e. of the uncertainty, as quantified by the ratio $\sigma_{Y^c}^2(\mathbf{x})/\sigma_Y^2(\mathbf{x}) \leqslant 1$. Ideally, if the ratio is close to zero, the inversion yields a deterministic field $Y^c(\mathbf{x}) \approx \langle Y^c(\mathbf{x})\rangle$. To determine the impact of measurement point density Dagan (1985, Fig. 2) considered a square grid of side a and derived the variance reduction factor at the center of a square as function of the ratio a/I for conditioning by either measured Y or H. The striking result was that unlike conditioning by Y for which $\sigma_{Y^c}^2(\mathbf{x})/\sigma_Y^2(\mathbf{x})$ tends to zero with $a/I \to 0$, even for a very dense grid ($a/I \ll 1$) head measurements could reduce the variance ratio to no less than 0.30, a result in line with findings in the literature on the limited effect of head measurements (see e.g. Dagan, 1989).

The procedure could be applied in principle to the oscillatory well

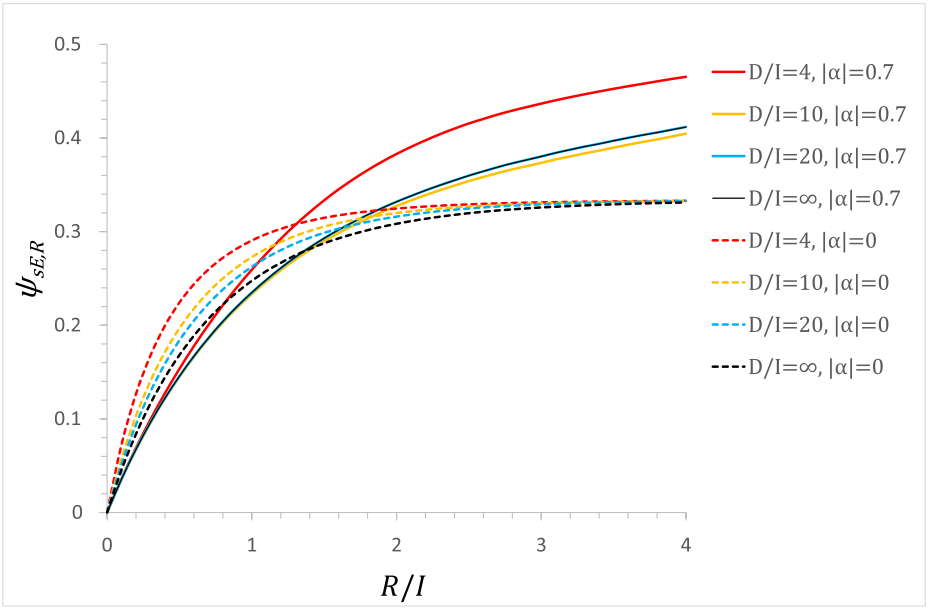

Fig. 7. The function ψ (real part) for a point source (exponential auto-correlation) at the mid-point of a confined aquifer as function of dimensionless horizontal distance for varying aquifer thickness (D/I).

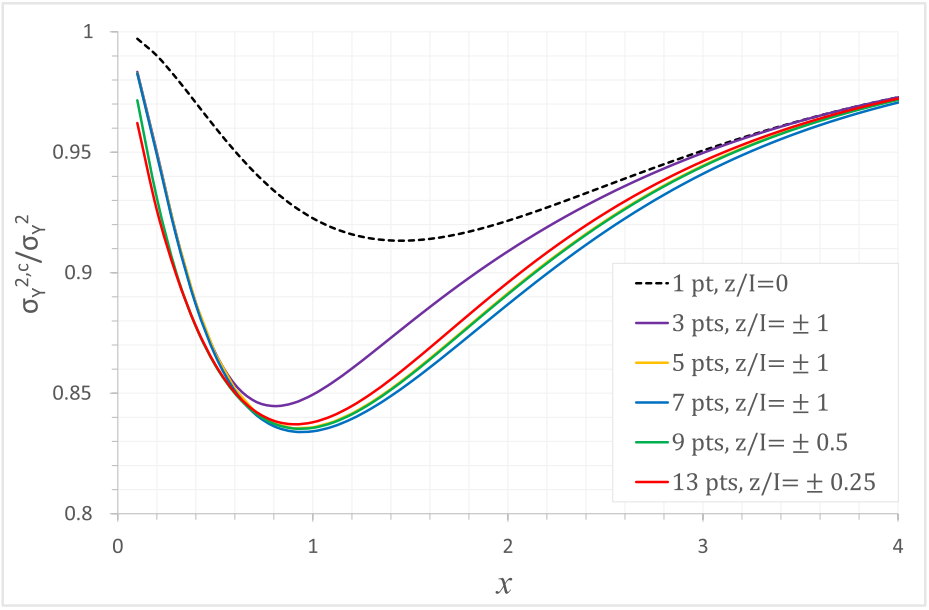

Fig. 8. The impact of head measurement conditioning on reduction of $Y = lnK$ variance for exponential auto-correlation as function of dimensionless horizontal distance from the measurement points. Number and separation distance of measurement points along z are indicated in the legend.

flow. However, while the non-stationary cross-covariance C_{YH} could be determined by two quadratures for a point source and isotropic Y field, the head covariance $C_H(\mathbf{x}, \mathbf{x}')$ appearing in (16) needs six quadratures and its computation was not undertaken at present.

Still, to get an indication about the impact of head measurements upon identification of Y^c we consider 3D flow of mean gradient $J = |dH_0/dr|$ in the horizontal direction assumed to be locally uniform and use the analytical expressions C_{YH} and C_H derived by Dagan (1989, Eqs. (3.7.8), (3.7.12), Figs. 3.7.3, 3.7.4) for isotropic media in order to derive the variance reduction at points in the neighborhood of a row of head measurement points along the vertical. This may provide an indication of the impact of head conditioning for oscillatory well flow. To be more specific, we have considered a row of an even number of measurement points at $x = 0$, $y = 0$, $|z_M|/I = \sum_{m=0}^{M} m(\Delta z/I)$ with $M = 0, 1, 2, \ldots$ and variable $\Delta z/I$ and computed the variance reduction $\sigma_Y^{2,c}(|x|, 0, 0)/\sigma_Y^2(|x|, 0, 0)$ along a horizontal line $x > 0$ (the results is symmetrical for $x < 0$) through the origin (Fig. 8). Such an analysis was not conducted before for 3D flow.

For a single measurement point (17) leads to $\mu_1 = C_{YH}(x, 0, 0)/\sigma_H^2$ and $\sigma_Y^{2,c}/\sigma_Y^2 = 1 - C_{YH}^2(x, 0, 0)/\sigma_H^2$ which is represented by the dashed line in Fig. 8. It is seen that the graph of $C_{YH}^2(x, 0, 0)/\sigma_H^2$ is similar to that of $C_{YH}(x, 0, 0)$ (Dagan, 1989, Fig. 3.7.3): $C_{YH} = 0$ for $x/I = 0$ and $x/I \gg 1$ and has a minimum around $x/I \cong 1.4$. Consequently, there is no variance reduction at the origin and far from the head measurement point, while the maximal effect is $(\sigma_Y^{2,c}/\sigma_Y^2)_{\min} \cong 0.92$ at $x/I \cong 1.4$. Increasing the number of measurement points (Fig. 8) with $\Delta z/I = 1$ leads to a similar behavior though the variance is further reduced and it reaches the maximal reduction $(\sigma_Y^{2,c}/\sigma_Y^2)_{\min} \cong 0.83$. This saturation value is practically reached for $M = 2$ (5 conditioning points). A slightly, negligible, larger reduction is achieved for smaller $\Delta z/I = 0.5, 0.25$ for a larger number of conditioning points. Since the conditional variance is reduced to zero at a point of conductivity measurement and increases with distance in a zone of a few integral scales, the conclusion is that head measurements along a vertical line in 3D are much less effective than measurements of Y in reducing the uncertainty of the identified Y^c field.

We plan to extend the computations to the oscillatory well flow configuration in the future. Still the results for uniform flow indicate that the stochastic inversion by co-kriging (similar to tomography) based on head measurements alone along piezometers is quite ineffective in identifying Y.

6. Application to Boise aquifer test

The Boise aquifer continuous pumping tests as well as their interpretations are discussed in a number of publications (e.g. Barrash and Clemo, 1999; Barrash et al., 2006; Barrash and Clemo, 2002; Cardiff et al., 2012, 2013b). The oscillatory test was analyzed by Rabinovich et al. (2015), which is the basis of the present discussion. One of their main results is summarized in their Fig. 7a displaying the dependence of the equivalent conductivity K_{eq} on the period T. The adopted definition of K_{eq} and s_{eq} is the one of a homogeneous and isotropic aquifer with same geometry and given Q_w, ω, which leads to a solution of the head field which provides a best approximation of the measured profiles of the head amplitude and phase in a few piezometers. It is reminded that the homogeneous and isotropic aquifer solution for a point source (see Eq. (5)) is given by

$$H_{s,\text{hom}} = (Q_w/K_{eq})(4\pi r)^{-1/2}\exp[-(i\omega s_{eq} r/K_{eq})]$$
$$\text{with } r = [x^2 + y^2 + (z - z')^2]^{1/2}, \tag{18}$$

while for the pumping well H_{hom} is obtained by integrating over z' along the well, supplemented by the images across the boundaries. After identifying the storativity s_{eq} from the phase analysis, Rabinovich et al. (2015) determined K_{eq} by minimizing the difference between $|H_{\text{hom}}|$ and the measured head amplitude profiles in a few piezometers.

Toward generalization of the procedure for heterogeneous aquifers along the present study, we shall recall a few relevant features of the Boise aquifer test. Thus pumping took place along 3 segments of length $L = 1$ m at 3 different elevations in the pumping well. The oscillating head response was measured along the selected 3 piezometers at distances $R = 3.75$ m, 6.26 m, 10.55 m with ports at a distance of $\Delta z = 2$ m along them (the setup is depicted in of Rabinovich et al. (2015, Fig. 2)). Examination of the head amplitude profiles indicate that only some of them resemble the theoretical ones either for homogeneous or the mean head for heterogeneous. These are the profiles associated with the mid interval in the pumping well for which $D_w = 8$ m (the 9 profiles for the three piezometers and 3 frequencies are represented in Fig. 5a of Rabinovich et al. (2015)) and we shall carry out the analysis for these ones solely. The tests for these profiles were carried out at 3 frequencies $\omega = 2\pi/T$, with $T = 28.5$, 40, 69 s, respectively.

The values of K_{eq} identified by Rabinovich et al. (2015) and

represented in their Fig. 7a are $K_{eq} = 3.8 \times 10^{-4}$, 3.7×10^{-4}, 3.8×10^{-4} m/s for $T = 28.5$, 40, 69 s, respectively. This was achieved by using the experimental head profiles $|H|$ as function of z represented in their Fig. 5a for the 3 values of R and the 3 values of T, altogether 9 profiles. For each T, K_{eq} was determined by a best fit of the theoretical and measured profiles simultaneously for the 3 piezometers differing in R. The closeness of the resulting values of K_{eq} is indeed an indication that the frequency impact is well accounted for by the theory in the specific range of T. The identified $s_{eq} \cong 10^{-5}\ \mathrm{m}^{-1}$ varies also little with T (Rabinovich et al., 2015, Fig. 5b).

We proceed now with the use of same 9 measured head profiles for the heterogeneous aquifer analysis, by a similar procedure of best fit of the theoretical mean head amplitude $\langle|H|\rangle = |H_0| + \langle|H_2|\rangle = |H_0|(1 + \sigma_Y^2\psi_{E,R})$ and measurements.

It is important to mention that the length L of the pumping intervals relative to the vertical integral scale I_v (which was found to be around 1.2 m in previous investigations of the aquifer) is much smaller than the one required in order to exchange the mean spatial $\overline{K}$ along the well with K_A, as assumed in the present theoretical derivations. Furthermore, even if one would try to condition on the actual $\overline{K}$, we are not aware of available information about K distribution along the pumping well. We are inclined to assume that $\overline{K}$ for the middle interval is closer to K_A than for the others. Besides this assumption, comparing the one realization limited set of measurements with the theoretical head ensemble mean is quite far reaching and the analysis shall be regarded as an illustrative one.

Unlike the model of a homogeneous aquifer in which the only unknown parameters were s_{eq} and K_{eq}, by adopting the assumption of isotropy used by Rabinovich et al. (2015), the theoretical mean amplitude $\langle|H|\rangle$ depends on s, K_G, σ_Y^2 and I. Since the phase of $\langle H\rangle$ was shown to be insensitive to heterogeneity, we adopt the value of $s = s_{eq} \cong 10^{-5}\ \mathrm{m}^{-1}$ identified by Rabinovich et al. (2015, Fig. 7b) based on phase analysis for a homogeneous aquifer. Due to the relatively small difference between the theoretical head profiles for a homogeneous aquifer and a heterogeneous one (see Fig. 5), there are problems of identifiability of the 3 remaining parameters. We limited therefore the search to the integral scale I, after adopting values obtained independently by past analysis for the other two parameters; thus, we took $\sigma_Y^2 \simeq 0.5$ cited by Rabinovich et al. (2015). This choice is motivated by practical considerations: while K_G and σ_Y^2 can be determined by analyzing samples of K along a few vertical profiles, identification of I requires a variogram analysis in the horizontal direction which is based on a large number of observation wells and is much more difficult to achieve.

Subsequently the analysis was conducted in the spirit of Rabinovich et al. (2015) as follows. By plugging in the expression of the theoretical mean amplitude $\langle|H|\rangle = |H_0| + \langle|H_2|\rangle = |H_0|(1 + \sigma_Y^2\psi_E)$ pertaining to the Boise data, i.e. the pumping interval of length $L = 1$ m in the confined aquifer of thickness $D = 19$ m , centered at an elevation of $D_w - L/2 = 10$ m beneath the top (Fig. 1), the aforementioned values of s and σ_Y^2, $\langle|H|\rangle$ becomes a function of T, R, z and K_G, I. We have derived the dependence of I upon K_G by a best fit of the theoretical and measured profiles for the 3 values of R simultaneously and for each T; the result is presented in Fig. 9.

It is seen that the 3 graphs display similar trends, but with a difference between the largest $T = 69$ s and the other two. However, the maximal range $2.6 \times 10^{-4}\ \mathrm{m/s} \lesssim K_G \lesssim 3.4 \times 10^{-4}$ m/s is relatively narrow compared with values of K derived by different methods as summarized in Table 2 in Barrash and Cardiff (2013). Furthermore, if we regard $K_{eq} \cong 3.8 \times 10^{-4}$ m/s identified by Rabinovich et al. (2015) as an effective value K_{ef} and assume that it is related to K_G by the first-order approximation for a stratified formation (due to large weight of the head measurements in the closest piezometer at $R = 3.75$ m), $K_{ef} = K_A = K_G(1 + \sigma_Y^2/2)$, we arrive at $K_G \cong 3 \times 10^{-4}$ m/s. This value is close to the one determined in the past by the tracer test (Nelson, 2007) and confirmed by the hydraulic tomography (Cardiff et al., 2012). For this value the corresponding range of integral scales in Fig. 9 is $7m \lesssim I \lesssim 12$ m, which is compatible with those determined independently by Cardiff and Barrash (2011) and Barrash and Cardiff (2013). It is also seen that the identified I value is quite sensitive to that of K_G and the latter should be based on analysis of measured K profiles rather than indirectly from hydraulic tests. In any case, while the identification of the range of K_G values is quite robust and in agreement with the analysis based on the homogeneous aquifer model, for the present conditions that of I is subjected to uncertainty.

We have also plotted in Fig. 10 the measured $|H|$ profiles (identical to those of Rabinovich et al. (2015, Fig. 5a)), the theoretical ones $|H_o|$ and $|H|$ as well as the ones pertaining to a homogeneous aquifer of K_{eq}. It is emphasized that the best fit leading to K_{eq} was carried out simultaneously for the 3 values of R, and not just $R = 3.75$ m as presented. As it is expectable, the theoretical $|H|$ and those based on homogeneous of K_{eq} are very close. In contrast the difference between $|H_o|$ and $|H|$ illustrate the impact of heterogeneity.

7. Summary and conclusions

The present study is a direct continuation of the paper by Dagan and Rabinovich (2014), which derived the spatial distribution of the head phasor for a partially penetrating oscillatory pumping well in a homogeneous and confined aquifer, of constant conductivity K and specific storativity s. The present paper extends the solution to a spatially variable $Y = \ln K$, which in the stochastic context is regarded as a realization of a random and stationary space function. The latter is parametrized by the geometric mean K_G, the variance σ_Y^2 and two-point covariance (exponential or Gaussian) characterized by the horizontal and vertical integral scales I and I_v, respectively. The solution for the phasor expected value $\langle H\rangle$ is obtained by a first order approximation in σ_Y^2, applicable to weakly heterogeneous aquifers. The solution is expressed by $\langle H\rangle = H_0 + \langle H_2\rangle = H_0(1 + \sigma_Y^2\psi)$, where H_0 pertains to a homogeneous aquifer of conductivity K_G, while the correction $\psi = \langle H_2\rangle/H_0$ depends on the spatial coordinates as well as on $\omega = 2\pi/T$, s, K_G, I and $f = I_v/I$, where T is the period.

The main theoretical result is the derivation of the function ψ in terms of a few quadratures by using the basic solution for a point source in an unbounded domain. Its integration along the length of the screen of the pumping well supplemented by appropriate images across the assumed impervious boundaries leads to the complete expression of $\langle H\rangle$.

A first finding was that ψ has a minor effect upon the phase of $\langle H\rangle$ and therefore the diffusivity can be determined from that of H_0, by using the homogeneous aquifer solution precisely like in Rabinovich et al. (2015). The study was focused subsequently on the amplitude $\langle|H|\rangle = |H_0||(1 + \sigma_Y^2\psi_R)|$; the behavior of the real part ψ_R (which contributes to the amplitude at first order) as a function of distance from the well was explored for different configurations. Generally, the solution pertains to a homogeneous aquifer of conductivity K_A (the arithmetic mean) near the well, which is the assumed boundary condition, and it varies with distance tending to the solution of a homogeneous aquifer of effective conductivity far from the well. However, due to the fast decay of $|H_0|$ with distance from the well for not very large periods, the far field behavior may not be reached.

As a by-product it is possible to derive the first order approximation of the two point head-logconductivity and head covariances. These can be used in order to condition the values of Y upon measurements of H by co-kriging, in the spirit of the hydraulic tomography. This task is outlined but not undertaken here. To get an indication of the impact of measured H values upon the uncertainty of Y, an analysis is carried out for the first time for steady 3D uniform flow. The result is that H measurements have little impact on reducing the uncertainty of conditioned Y. A future study for well flow shall elucidate the issue for non-uniform flow.

Finally, we have applied the theoretical results to the Boise aquifer test by demanding that the amplitude of the measured H in 3 selected profiles is equal to the one based on the theoretical mean head. By assuming known values of previously determined s, K_{eq} and σ_Y^2 we have been able to identify the integral scale I for an isotropic medium as

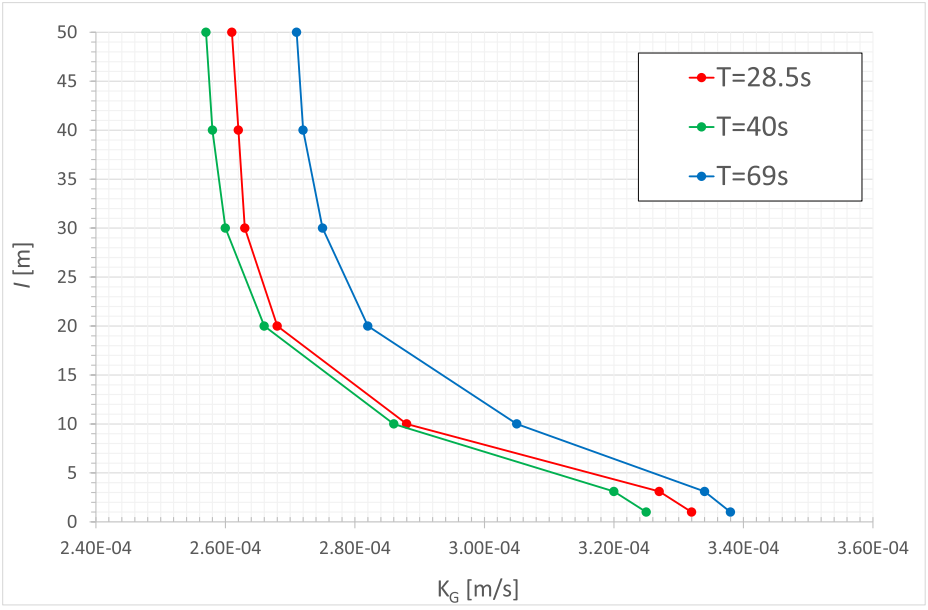

Fig. 9. The dependence of the integral scale on the conductivity geometric mean for three periods by a best fit of the theoretical and measured head profiles from Boise aquifer tests.

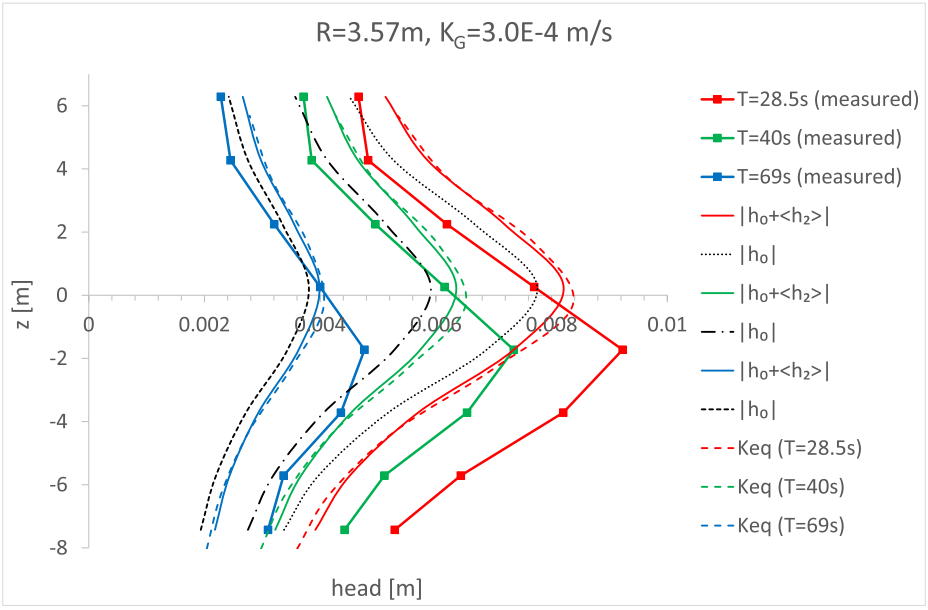

Fig. 10. Head profiles: measured, homogeneous aquifer of K_{eq}, theoretical (second-order) and zero-order approximation (Boise aquifer tests).

function of the period T. The values are in a range compatible with independent previously derived values.

In spite of the many simplifying assumptions, we conclude that the stochastic approach allows to gain understanding of the dependence of the head field on the various parameters characterizing the oscillatory pumping and the aquifer. The application to Boise aquifer test and inversion leads to reasonable range of values of the identified geometric mean K_G, while that of the integral scale I is quite sensitive to the choice of K_G.

Declaration of interests

The authors declare that they have no known competing financial interests or personal relationships that could have appeared to influence the work reported in this paper.

Acknowledgements

The paper is part of the PhD study carried out by the first author at and supported by the School of Mechanical Engineering, Faculty of Engineering, Tel Aviv University. The advice provided by Dr. Amir Paster is acknowledged with gratitude.

Appendix A. Derivation of $\langle h_{2s} \rangle$

With dimensionless head $h = h_{0s} + h_{1s} + h_{2s}$ and define the dimensionless parameter $\alpha = \frac{\gamma^2}{K_G} I^2$. Assuming point source, the series of Poisson equations can be re-written as

$$\alpha h_{0s} - \nabla^2 h_{0s} = \delta(z - z')\delta(x)\delta(y) \tag{A.1}$$

$$\alpha h_{1s} - \nabla^2 h_{1s} = \nabla Y' \cdot \nabla h_{0s} + \alpha Y' h_{0s} \tag{A.2}$$

$$\alpha h_{2s} - \nabla^2 h_{2s} = \nabla Y' \cdot \nabla h_{1s} + \alpha Y' h_{1s} - \alpha \frac{Y'^2}{2} h_{0s} \tag{A.3}$$

Using the Green's function, the solutions to the Poisson equation are given by:

$$h_{0s}(\mathbf{x}) = G(\mathbf{x}) = -\frac{e^{-\sqrt{\alpha}|\mathbf{x}|}}{4\pi|\mathbf{x}|} \tag{A.4}$$

$$\begin{aligned} h_{1s}(\mathbf{x}) =& -\int d\mathbf{x}' G(\mathbf{x}-\mathbf{x}')[\nabla Y'(\mathbf{x}')\cdot\nabla h_{0s}(\mathbf{x}') + \alpha Y'(\mathbf{x}') h_{0s}(\mathbf{x}')] \\ =& -\int d\mathbf{x}' G(\mathbf{x}-\mathbf{x}')[\nabla Y'(\mathbf{x}')\cdot\nabla h_{0s}(\mathbf{x}')] \\ & - \alpha \int d\mathbf{x}' G(\mathbf{x}-\mathbf{x}') Y'(\mathbf{x}') h_{0s}(\mathbf{x}') \end{aligned} \tag{A.5}$$

$$\begin{aligned} h_{2s}(\mathbf{x}) =& -\int d\mathbf{x}'' G(\mathbf{x}-\mathbf{x}'')[\nabla Y'(\mathbf{x}'')\cdot\nabla h_{1s}(\mathbf{x}'') + \alpha Y'(\mathbf{x}'') h_{1s}(\mathbf{x}'') \\ & - \alpha \frac{[Y'(\mathbf{x}'')]^2}{2} h_{0s}\Big] \\ =& -\int d\mathbf{x}'' G(\mathbf{x}-\mathbf{x}'')[\nabla Y'(\mathbf{x}'')\cdot\nabla h_{1s}(\mathbf{x}'')] \\ & - \alpha \int d\mathbf{x}'' G(\mathbf{x}-\mathbf{x}'') Y'(\mathbf{x}'') h_{1s}(\mathbf{x}'') \\ & + \frac{\alpha}{2} \int d\mathbf{x}'' G(\mathbf{x}-\mathbf{x}'')[Y'(\mathbf{x}'')]^2 h_{0s}(\mathbf{x}'') \end{aligned} \tag{A.6}$$

Plug h_{1s} (A.5) into h_{2s} (A.6)

$$\begin{aligned} h_{2s}(\mathbf{x}) =& \int d\mathbf{x}'' G(\mathbf{x}-\mathbf{x}'') \frac{\partial Y'(\mathbf{x}'')}{\partial x_j''} \int d\mathbf{x}' \frac{\partial Y'(\mathbf{x}')}{\partial x_i'} \frac{\partial h_{0s}(\mathbf{x}')}{\partial x_i'} \frac{\partial G(\mathbf{x}''-\mathbf{x}')}{\partial x_j''} \\ & + \alpha \int d\mathbf{x}'' G(\mathbf{x}-\mathbf{x}'') \frac{\partial Y'(\mathbf{x}'')}{\partial x_j''} \int d\mathbf{x}' Y'(\mathbf{x}') h_{0s}(\mathbf{x}') \frac{\partial G(\mathbf{x}''-x')}{\partial x_j''} \\ & + \alpha \int d\mathbf{x}'' G(\mathbf{x}-\mathbf{x}'') Y'(\mathbf{x}'') \int d\mathbf{x}' \frac{\partial Y'(\mathbf{x}')}{\partial x_i'} \frac{\partial h_{0s}(\mathbf{x}')}{\partial x_i'} G(\mathbf{x}''-\mathbf{x}') \\ & + \alpha^2 \int d\mathbf{x}'' G(\mathbf{x}-\mathbf{x}'') Y'(\mathbf{x}'') \int d\mathbf{x}' G(\mathbf{x}''-\mathbf{x}') Y'(\mathbf{x}') h_{0s}(\mathbf{x}') \\ & + \frac{\alpha}{2} \int d\mathbf{x}'' G(\mathbf{x}-\mathbf{x}'')[Y'(\mathbf{x}'')]^2 h_{0s}(\mathbf{x}'') \\ =& \, h_{211} + h_{212} + h_{221} + h_{222} + h_{23} \end{aligned} \tag{A.7}$$

By the change of variable $\mathbf{y} = \mathbf{x}'' - \mathbf{x}'$, and note that $\frac{\partial^2 \rho(\mathbf{x}''-\mathbf{x}')}{\partial x_i' \partial x_j''} = -\frac{\partial^2 \rho(\mathbf{y})}{\partial y_i \partial y_j}$, after some manipulations we arrive at the expressions for ensemble averaging of all 5 component terms as below:

$$\begin{aligned} \frac{\langle h_{211}(\mathbf{x})\rangle}{\sigma_Y^2} =& \int d\mathbf{x}' \int d\mathbf{x}'' \frac{\partial^2 \rho(\mathbf{x}''-\mathbf{x}')}{\partial x_i' \partial x_j''} \frac{\partial G(\mathbf{x}')}{\partial x_i'} \frac{\partial G(\mathbf{x}''-\mathbf{x}')}{\partial x_j''} G(\mathbf{x}''-\mathbf{x}) \\ =& -\int d\mathbf{y} \frac{\partial^2 \rho(\mathbf{y})}{\partial y_i \partial y_j} \frac{\partial G(\mathbf{y})}{\partial y_j} \int d\mathbf{x}' \frac{\partial G(\mathbf{x}')}{\partial x_i'} G(\mathbf{x}-\mathbf{x}'-\mathbf{y}) \\ =& \int d\mathbf{y} \frac{d^2\rho(y)}{dy^2} \frac{(\mathbf{x}\cdot\mathbf{y}-y^2)}{y\,|\,\mathbf{x}-\mathbf{y}|} \frac{e^{-y\sqrt{\alpha}}(1+y\sqrt{\alpha})}{4\pi y^2} \left[\frac{e^{-\sqrt{\alpha}|\mathbf{x}-\mathbf{y}|}}{8\pi}\right] \\ \frac{\langle h_{212}(\mathbf{x})\rangle}{\sigma_Y^2} =& \alpha \int d\mathbf{x}'' \int d\mathbf{x}' \frac{\partial \rho(\mathbf{x}''-\mathbf{x}')}{\partial x_j''} G(\mathbf{x}-\mathbf{x}'') G(\mathbf{x}') \frac{\partial G(\mathbf{x}''-\mathbf{x}')}{\partial x_j''} \\ =& \alpha \int d\mathbf{y} \frac{y_j}{y} \frac{d\rho(y)}{dy} \frac{y_j}{y} \frac{dG(y)}{dy} \int d\mathbf{x}' G(\mathbf{x}') G(\mathbf{x}-\mathbf{x}'-\mathbf{y}) \\ =& \int d\mathbf{y} \frac{d\rho(\mathbf{y})}{dy} \frac{\sqrt{\alpha} e^{-y\sqrt{\alpha}}(1+y\sqrt{\alpha})}{4\pi y^2} \left[\frac{e^{-\sqrt{\alpha}|\mathbf{x}-\mathbf{y}|}}{8\pi}\right] \\ \frac{\langle h_{221}(\mathbf{x})\rangle}{\sigma_Y^2} =& \alpha \int d\mathbf{x}'' \int d\mathbf{x}' \frac{\partial \rho(\mathbf{x}''-\mathbf{x}')}{\partial x_i'} G(\mathbf{x}-\mathbf{x}'') \frac{\partial G(\mathbf{x}')}{\partial x_i'} G(\mathbf{x}''-\mathbf{x}') \\ =& -\alpha \int d\mathbf{y} \frac{y_i}{y} \frac{d\rho(y)}{dy} G(\mathbf{y}) \int d\mathbf{x}' \frac{\partial G(\mathbf{x}')}{\partial x_i'} G(\mathbf{x}-\mathbf{x}'-\mathbf{y}) \\ =& -\int d\mathbf{y} \frac{1}{y} \frac{d\rho(\mathbf{y})}{dy} \left(\frac{\alpha e^{-y\sqrt{\alpha}}}{4\pi y}\right) \frac{(\mathbf{x}\cdot\mathbf{y}-y^2)}{|\mathbf{x}-\mathbf{y}|} \left[\frac{e^{-\sqrt{\alpha}|\mathbf{x}-\mathbf{y}|}}{8\pi}\right] \\ \frac{\langle h_{222}(\mathbf{x})\rangle}{\sigma_Y^2} =& \alpha^2 \int d\mathbf{x}'' \int d\mathbf{x}' \rho(\mathbf{x}''-\mathbf{x}') G(\mathbf{x}-\mathbf{x}'') G(\mathbf{x}''-\mathbf{x}') G(\mathbf{x}') \\ =& \alpha^2 \int d\mathbf{y} \rho(\mathbf{y}) G(\mathbf{y}) \int d\mathbf{x}' G(\mathbf{x}') G(\mathbf{x}-\mathbf{x}'-\mathbf{y}) \\ =& -\int d\mathbf{y} \rho(\mathbf{y}) \frac{\alpha^{3/2} e^{-y\sqrt{\alpha}}}{4\pi y} \left[\frac{e^{-\sqrt{\alpha}|\mathbf{x}-\mathbf{y}|}}{8\pi}\right] \\ \frac{\langle h_{23}(\mathbf{x})\rangle}{\sigma_Y^2} =& \frac{\alpha}{2} \int d\mathbf{x}'' G(\mathbf{x}-\mathbf{x}'') G(\mathbf{x}'') = \frac{\alpha}{2} I(\mathbf{x}) = \frac{\sqrt{\alpha}}{2} \left[\frac{e^{-\sqrt{\alpha}|\mathbf{x}|}}{8\pi}\right] \end{aligned}$$

Combining all 5 terms and simplifying to arrive at the final expression for $\langle h_{2s} \rangle$

$$\begin{aligned} \frac{\langle h_{2s}(\mathbf{x})\rangle}{\sigma_Y^2} =& \left\{ \int d\mathbf{y} \left[\frac{d^2\rho(y)}{dy^2} \frac{(1+y\sqrt{\alpha})(\mathbf{x}\cdot\mathbf{y}-y^2)}{y^2\,|\,\mathbf{x}-\mathbf{y}|} + \frac{d\rho(y)}{dy} \frac{\sqrt{\alpha}(1+y\sqrt{\alpha})}{y} \right.\right. \\ & \left.\left. + \frac{d\rho(y)}{dy} \frac{\alpha(\mathbf{x}\cdot\mathbf{y}-y^2)}{|\mathbf{x}-\mathbf{y}|} - \rho(y)\alpha^{3/2} \right] \left[\frac{e^{-y\sqrt{\alpha}}}{4\pi y}\right] \left[\frac{e^{-\sqrt{\alpha}|\mathbf{x}-\mathbf{y}|}}{8\pi}\right] \right\} \\ & + \frac{\sqrt{\alpha}}{2} \left[\frac{e^{-\sqrt{\alpha}|\mathbf{x}|}}{8\pi}\right] \end{aligned} \tag{A.8}$$

Plug in expressions of Gaussian and exponential auto-correlation for ρ respectively

$$\begin{aligned} \psi_{sG}(\alpha, r) =& \int_0^\infty dy \int_{-1}^1 d\lambda \frac{e^{\frac{-\pi}{4}y^2 - \sqrt{\alpha}\left(y+\sqrt{r^2+y^2-2ry\lambda}\right)}}{64\pi\sqrt{r^2+y^2-2ry\lambda}} [-\pi^2 y^2 (1+y\sqrt{\alpha})(y-r\lambda) \\ & - 2\pi(-1 - y\sqrt{\alpha} + \alpha y^2)(y-r\lambda) - 2\pi y\sqrt{\alpha}\sqrt{r^2+y^2-2ry\lambda} \\ & - 2\pi y^2 \alpha \sqrt{r^2+y^2-2ry\lambda} - 4y\alpha^{3/2}\sqrt{r^2+y^2-2ry\lambda}\,] \\ & + \frac{\sqrt{\alpha} e^{-\sqrt{\alpha} r}}{16\pi} \end{aligned} \tag{A.9}$$

$$\begin{aligned} \psi_{sE}(\alpha, r) =& \int_0^\infty dy \int_{-1}^1 d\lambda \frac{e^{-y-\sqrt{\alpha}\left(y+\sqrt{r^2+y^2-2ry\lambda}\right)}}{32\pi^2\sqrt{r^2+y^2-2ry\lambda}} [1 + y(\alpha+\sqrt{\alpha})]\lambda \\ & \cdot (r\lambda - y - \sqrt{\alpha}\sqrt{r^2+y^2-2ry\lambda}) + \frac{\sqrt{\alpha} e^{-\sqrt{\alpha} r}}{16\pi} \end{aligned} \tag{A.10}$$

References

Bakhos, T., Cardiff, M., Barrash, W., Kitanidis, P.K., 2014. Data processing for oscillatory pumping tests. J. Hydrol. 511, 310–319.

Barrash, W., Cardiff, M., 2013. Hydraulic Conductivity Distribution from Multi-level Slug Tests and Multivariate Facies Associations in a Conglomeratic Fluvial Aquifer, Boise Hydrogeophysical Research Site: Technical Report BSU CGISS, 13–03. Tech. Rep. August.

Barrash, W., Clemo, T., 1999. Boise Hydrogeophysical Research Site (BHRS): Objectives, design, initial geostatistical results. In: Proceedings of SAGEEP99, The Symposium on the Application of Geophysics to Engineering and Environmental Problems, March 14–18, 1999, Oakland, CA. pp. 389–398.

Barrash, W., Clemo, T., 2002. Hierarchical geostatistics and multifacies systems – Boise Hydrogeophysical Research Site, Boise, Idaho. Water Resour. Res. 38 (10), 1196.

Barrash, W., Clemo, T., Fox, J.J., Johnson, T.C., 2006. Field, laboratory, and modeling investigation of the skin effect at wells with slotted casing, Boise Hydrogeophysical Research Site. J. Hydrol. 326 (1–4), 181–198.

Cardiff, M., Bakhos, T., Kitanidis, P.K., Barrash, W., 2013a. Aquifer heterogeneity characterization with oscillatory pumping: sensitivity analysis and imaging potential. Water Resour. Res. 49 (9), 5395–5410.

Cardiff, M., Barrash, W., 2011. 3-D transient hydraulic tomography in unconfined aquifers with fast drainage response. Water Resour. Res. 47 (12).

Cardiff, M., Barrash, W., 2015. Analytical and semi-analytical tools for the design of oscillatory pumping tests. Groundwater 53 (6), 896–907.

Cardiff, M., Barrash, W., Kitanidis, P.K., 2012. A field proof-of-concept of aquifer imaging using 3-D transient hydraulic tomography with modular, temporarily-emplaced equipment. Water Resour. Res. 48 (5).

Cardiff, M., Barrash, W., Kitanidis, P.K., 2013b. Hydraulic conductivity imaging from 3-D transient hydraulic tomography at several pumping/observation densities. Water Resour. Res. 49 (11), 7311–7326.

Carrera, J., Alcolea, A., Medina, A., Hidalgo, J., Slooten, L.J., 2005. Inverse problem in hydrogeology. Hydrogeol. J. 13 (1), 206–222.

Carslaw, H.D., Jaeger, J.C., 1959. Conduction of heat in solids, Vol. 1.

Dagan, G., 1985. Stochastic modeling of groundwater flow by unconditional and conditional probabilities: the inverse problem. Water Resour. Res. 21 (1), 65–72.

Dagan, G., 1989. Flow and Transport in Porous Formations. Springer-Verlag GmbH & Co, KG.

Dagan, G., Lessoff, S.C., 2011. Flow to partially penetrating wells in unconfined heterogeneous aquifers: Mean head and interpretation of pumping tests. Water Resour. Res. 47 (6).

Dagan, G., Rabinovich, A., 2014. Oscillatory pumping wells in phreatic, compressible and homogeneous aquifers. Water Resour. Res. 50 (8), 7058–7066.

Firmani, G., Fiori, A., Bellin, A., 2006. Three-dimensional numerical analysis of steady state pumping tests in heterogeneous confined aquifers. Water Resour. Res. 42 (3), 1–10.

Gelhar, L.W., Axness, C.L., 1983. Three-dimensional stochastic analysis of macrodispersion in aquifers. Water Resour. Res. 19 (1), 161.

Gottlieb, J., Dietrich, P., 1995. Identification of the permeability distribution in soil by hydraulic tomography. Inverse Prob. 11 (2), 353.

Guiltinan, E., Becker, M.W., 2015. Measuring well hydraulic connectivity in fractured bedrock using periodic slug tests. J. Hydrol. 521, 100–107.

Hollaender, F., Hammond, P.S., Gringarten, A.C., 2002. Harmonic testing for continuous well and reservoir monitoring. In: SPE Annual Technical Conference and Exhibition, San Antonio, Texas, U.S.A, 29 Sept-2 Oct.

Indelman, P., 2001. Steady-state source flow in heterogeneous porous media. Transp. Porous Media 45 (1), 105–127.

Indelman, P., Abramovich, B., 1994. Nonlocal properties of nonuniform averaged flows in

heterogeneous media. Water Resour. Res. 30 (12), 3385.
Indelman, P., Dagan, G., 2004. A note on well boundary condition for flow through heterogeneous formations. Water Resour. Res. 40 (3), W036011–W036017.
Kitanidis, P.K., 1996. On the geostatistical approach to the inverse problem. Adv. Water Resour. 19 (6), 333–342.
Marco, D.O., Andrea, Z., Fausto, C., 2018. Oscillatory pumping test to estimate aquifer hydraulic parameters in a bayesian geostatistical framework. Math. Geosci. 50 (2), 169–186.
McLaughlin, D., Townley, L.R., 1996. A reassessment of the groundwater inverse problem. Water Resour. Res. 32 (5), 1131–1161.
Nelson, G., 2007. Deterministic modeling of bromide tracer transport during the tracer/time-lapse radar imaging test at the Boise hydrogeophysical research site in August, 2001.
Rabinovich, A., Barrash, W., Cardiff, M., Hochstetler, D.L., Bakhos, T., Dagan, G., Kitanidis, P.K., 2015. Frequency dependent hydraulic properties estimated from oscillatory pumping tests in an unconfined aquifer. J. Hydrol. 531, 2–16.
Rabinovich, A., Dagan, G., Miloh, T., 2013. Effective conductivity of heterogeneous aquifers in unsteady periodic flow. Adv. Water Resour. 62, 317–326.
Rasmussen, T.C., Haborak, K.G., Young, M.H., 2003. Estimating aquifer hydraulic properties using sinusoidal pumping at the Savannah River site, South Carolina, USA. Hydrogeol. J. 11 (4), 466–482.
Renner, J., Messar, M., 2006. Periodic pumping tests. Geophys. J. Int. 167 (1), 479–493.
Severino, G., Santini, A., Sommella, A., 2008. Steady flows driven by sources of random strength in heterogeneous aquifers with application to partially penetrating wells. Stoch. Env. Res. Risk Assess. 22 (4), 567–582.
Yeh, T.-C.J., Liu, S., 2000. Hydraulic tomography: development of a new aquifer test method. Water Resour. Res. 36 (8), 2095.
Yeh, W.W., 1986. Review of parameter identification procedures in groundwater hydrology: the inverse problem. Water Resour. Res. 22 (2), 95–108.